

See discussions, stats, and author profiles for this publication at: <https://www.researchgate.net/publication/49687529>

# Role of the HAMP Domain Region of Sensory Rhodopsin Transducers in Signal Transduction

ARTICLE *in* BIOCHEMISTRY · FEBRUARY 2011

Impact Factor: 3.02 · DOI: 10.1021/bi101032a · Source: PubMed

---

CITATIONS

4

---

READS

26

## 3 AUTHORS, INCLUDING:



Ivan Gushchin

Forschungszentrum Jülich

16 PUBLICATIONS 70 CITATIONS

[SEE PROFILE](#)



Sergei Grudinin

National Institute for Research in Computer...

30 PUBLICATIONS 208 CITATIONS

[SEE PROFILE](#)

# Role of the HAMP Domain Region of Sensory Rhodopsin Transducers in Signal Transduction<sup>†</sup>

Ivan Yu. Gushchin,<sup>‡</sup> Valentin I. Gordeliy,<sup>‡,§</sup> and Sergei Grudinin\*,<sup>¶,||</sup>

<sup>‡</sup>Research-educational Centre “Bionanophysics”, Moscow Institute of Physics and Technology, 141700 Dolgoprudnyi, Russia, <sup>§</sup>Laboratoire des Protéines Membranaires, Institut de Biologie Structurale J.-P. Ebel, UMR5075 CEA-CNRS-UJF, 38027 Grenoble, France, and Institute of Structural Biology and Biophysics (ISB-2), Forschungszentrum Juelich, 52425 Juelich, Germany, and <sup>¶</sup>NANO-D, INRIA Grenoble-Rhone-Alpes Research Center, 38334 Saint Ismier Cedex, Montbonnot, France, and <sup>||</sup>CNRS, Laboratoire Jean Kuntzmann, BP 53, Grenoble Cedex 9, France

Received June 28, 2010; Revised Manuscript Received December 11, 2010

**ABSTRACT:** Archaea are able to sense light via the complexes of sensory rhodopsins I and II and their corresponding chemoreceptor-like transducers HtrI and HtrII. Though generation of the signal has been studied in detail, the mechanism of its propagation to the cytoplasm remains obscured. The cytoplasmic part of the transducer consists of adaptation and kinase activity modulating regions, connected to transmembrane helices via two HAMP (histidine kinases, adenylyl cyclases, methyl-accepting chemotaxis proteins, phosphatases) domains. The inter-HAMP region of *Natronomonas pharaonis* HtrII (NpHtrII) was found to be  $\alpha$ -helical [Hayashi, K., et al. (2007) *Biochemistry* 46, 14380–14390]. We studied the inter-HAMP regions of NpHtrII and other phototactic signal transducers by means of molecular dynamics. Their structure is found to be a bistable asymmetric coiled coil, in which the protomers are longitudinally shifted by  $\sim$ 1.3 Å. The free energy penalty for the symmetric structure is estimated to be 1.2–1.5 kcal/mol depending on the molarity of the solvent. Both flanking HAMP domains are mechanistically coupled to the inter-HAMP region and are asymmetric. The longitudinal shift in the inter-HAMP region is coupled with the in-plane displacement of the cytoplasmic part by 8.6 Å relative to the transmembrane part. The established properties suggest that (1) the signal may be transduced through the inter-HAMP domain switching and (2) the inter-HAMP region may allow cytoplasmic parts of the transducers to come sufficiently close to each other to form oligomers.

Archaea use light-sensing sensory rhodopsins (SRs)<sup>1</sup> I and II as positive and negative photoreceptors to move toward red light, which enables bacteriorhodopsin and halorhodopsin activity, and to avoid harmful near-UV light (1, 2). The signal from SR is relayed to the transducer protein (Htr), whose cytoplasmic tip forms a complex with CheA kinase and CheW adapter protein. CheA regulates phosphorylation of CheY, which controls the regime of rotation of the flagellar motor. Adaptation to a signal is regulated by proteins CheB and CheR, which are involved in adaptive methylation and demethylation of the transducers (3).

Sensory rhodopsins contain a covalently attached cofactor retinal, and their structure resembles that of bacteriorhodopsin (1, 2). In the membrane, receptors form 2:2 complexes with transducer proteins Htr (HtrI and HtrII). Both HtrI and HtrII

have a domain organization similar to that of bacterial chemo-receptors (see Figure 1). Transducers have a short unstructured cytoplasmic C-terminus, followed by transmembrane helix TM1, a chemotaxis receptor domain (only in HsHtrII), then another transmembrane helix TM2, two consecutive HAMP domains (4), separated by the inter-HAMP region, and the kinase control (KC) module with adaptational methylation sites. As opposed to Htr proteins, the chemotaxis proteins contain only one HAMP domain and no inter-HAMP region.

The crystallographic structure of NpSRII bound to transmembrane helices of NpHtrII (residues 23–82) is known for the ground, K, and M states (5, 6). The structure of the HAMP domains is represented well by the NMR structure of the HAMP domain of *Archeoglobus fulgidus* hypothetical protein Af1503 (7, 8). The NpHtrII fragment of residues 100–159 was shown to be trypsin-resistant, with the inter-HAMP region (residues 135–150) adopting an  $\alpha$ -helical structure (7, 9). The structure of the kinase control module of the homologous *Escherichia coli* serine chemoreceptor was also determined by X-ray crystallography (10). Other Htrs are highly homologous to NpHtrII and thus expected to adopt a similar conformation.

Several models of transduction of signals to the cytoplasmic domain were proposed. They include a pistonlike motion, a motion in the membrane plane, and rotation of transmembrane helix TM2 (3). There is crystallographic and cysteine-scanning mutagenesis evidence that in bacterial chemoreceptors the signal is conducted to the TM domain in a pistonlike fashion (11, 12). For NpHtrII, rotation by 15° and in-plane displacement by 0.9 Å of the

<sup>†</sup>This work was supported by the program “Chaires d’excellence” edition 2008 of ANR France, CEA(IBM)-HGF(FZJ) STC 5.1 specific agreement, the MC grant for training and career development of researchers (Marie Curie, FP7-PEOPLE-2007-1-1-ITN, project SBMPs), and an EC FP7 grant for the EDICT consortium (HEALTH-201924). This work was conducted in the framework of Russian State Contracts 02.740.11.0299, 02.740.11.5010, and P974 in the framework of activity 1.2.2 of the Federal Target Program “Scientific and academic research cadres of innovative Russia” for 2009–2013.

\*To whom correspondence should be addressed. Phone: +33 4 76 61 53 24. Fax: +33 4 76 15 36 23. E-mail: sergei.grudinin@inria.fr.

<sup>‡</sup>Abbreviations: HAMP domain, domain found in histidine kinases, adenylyl cyclases, methyl-accepting chemotaxis proteins, and phosphatases; AS1 and AS2, the first and the second  $\alpha$ -helices of the HAMP domain, respectively; KC, kinase control module; Np, *Natronomonas pharaonis*; Hs, *Halobacterium salinarum*; SR, sensory rhodopsin; Htr, sensory rhodopsin transducer; CC, coiled coil.

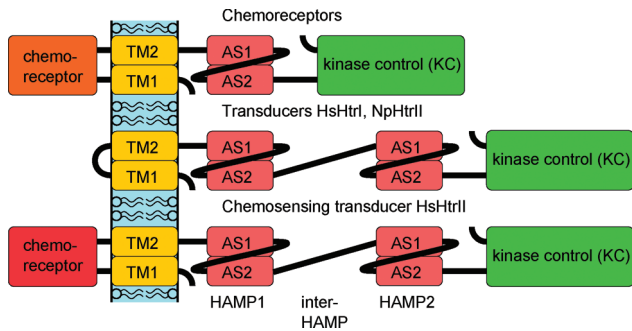


FIGURE 1: Domain architecture of bacterial chemoreceptors (top), the phototactic signal transducers HsHtrI and NpHtrII (middle), and the transducer and chemoreceptor HsHtrII (bottom). TM1 and TM2 are the transmembrane helices, and AS1 and AS2 are the helices of the HAMP domain. Chemoreceptor modules are colored differently as there is no sequence homology between them.

membrane interface part of helix TM2 were observed by crystallography (5). A gearboxlike model for the HAMP domain signal transduction was proposed on the basis of its NMR structure (8), but it is not backed up with any experimental evidence. Subsequently, a dynamic bundle model for HAMP domain function based on mutational experiments was proposed (13, 14). Finally, the crystallographic structure of three consecutive HAMP domains of *Pseudomonas aeruginosa* soluble receptor Aer2 led to a model of interconversion between the two HAMP domain conformational states (15). For the inter-HAMP region of NpHtrII, the role of a mechanical joint was proposed (9), though no details were provided.

Because the structure of the transducer transmembrane part is known (6), the structure of the HAMP domains should be similar to that of Af1503 (8), and the generation of the signal in the transmembrane region upon photoexcitation is established (5), we focused our study on the region of the HAMP domains. First, we analyzed the sequences of the proteins and found that their inter-HAMP regions are predicted to have an  $\alpha$ -helical structure and adopt a coiled-coil (CC) conformation. These coiled coils are unique because their hydrophobic residues are alanines. Moreover, charged residues surrounding the hydrophobic core are organized in such a way that an asymmetric configuration of protomers is possible. We also performed a molecular dynamics study of the NpHtrII inter-HAMP region. It shows a great instability of the symmetric conformation and spontaneous symmetry breaking with subsequent formation of an asymmetric configuration. As the primary structure of protomers is identical, two equally favorable asymmetric conformations are possible, which means that the inter-HAMP region may act as a switch that fixes the amplitude of the relative shift of the protomers, but not its sign. Finally, we studied the system of the two HAMP domains and the inter-HAMP region of NpHtrII by means of molecular dynamics. We found that the conventional structure model (8, 15) can be applied to these HAMP domains. However, it is important to note that they are asymmetrical as a consequence of coupling to the asymmetrical inter-HAMP region.

Obtained data suggest that the inter-HAMP region may play the role of a switch or of a passive rigid mechanical joint between two HAMP domains.

## MATERIALS AND METHODS

**Initial Data and Models.** All sequences and domain assignments were taken from reviewed UniProt database (16) records P33741 (HsHtrI), Q9HP81 (HsHtrII), and P42259 (NpHtrII).

The initial model for the NpHtrII  $\alpha$ -helical fragment of residues 135–150 was taken from Protein Data Bank (PDB) entry 2RM8 (9). The HAMP domain model for homology modeling was taken from PDB entry 2ASW (8). Initial models of  $\alpha$ -helices for which no structure was present were built using PyMOL (DeLano Scientific, Palo Alto, CA). For homology modeling of the NpHtrII HAMP domains, MODELLER (17) was used. Some energy minimizations and structure manipulations in the dihedral subspace were performed using the SAMSON symmetry module (18).

**Molecular Dynamics.** All molecular dynamics simulations were conducted using NAMD2 (19) with CHARMM27 parameters (20). Preparations of initial models and data analysis using our own tcl-scripts were performed in VMD (21). As a first step, hydrogen positions of a model in a vacuum were minimized for 50 standard NAMD minimization steps. This was followed by addition of a water box with a padding of 8 Å. Sodium and chloride ions were added at a total concentration of 0.5, 1, 2, or 4 M, accordingly, for different simulations, in such amounts that the system had zero total charge. Simulation in the water box was conducted with periodic boundary conditions. The water box was minimized for 50 steps and then was subjected to molecular dynamics for 1 ps, with protein atoms frozen. After that, the whole system was minimized for 1000 steps and then heated to 310 K in steps of 10 K and 0.1 ps per step. The integration time step was 2 fs, and the SHAKE algorithm was used to keep bonds between hydrogens and heavy atoms rigid. The temperature of 310 K was maintained with a Langevin thermostat with a damping coefficient of 5 ps<sup>-1</sup>. The pressure of 1 bar was maintained with a Langevin piston with the following parameters: period of 100 fs and decay of 50 fs. For electrostatic calculations, the particle-mesh Ewald method was used. Additional information about the model preparation and stability can be found in Table S1 of the Supporting Information.

**Longitudinal Shift Calculations.** For each frame of the MD trajectory, calculations were conducted as follows. First, the direction of each helix was determined as the main axis of its inertia tensor, along which the moment of inertia is minimal. Second, the CC axis was calculated as an average of directions of the two individual helices. Finally, the vector difference in the positions of the centers of mass of respective helices was projected on the CC axis to determine the relative shift of helices. For these calculations, only positions of the backbone atoms were used.

**Free Energy Calculations.** To determine the free energy of a system as a function of longitudinal shift, we used the umbrella sampling technique (22) followed by either the weighted histogram analysis method (WHAM) (23) or the multiple-Bennett acceptance ratio method (MBAR) (24). We used WHAM implementation by A. Grossfield (<http://membrane.urmc.rochester.edu/content/wham>, version 2.04) and MBAR implementation by J. Chodera and M. Shirts (<https://simtk.org/home/pymbar>).

Sampling positions along the longitudinal shift were -2.1, -1.4, -0.7, 0, 0.7, 1.4, and 2.1 Å with force constants of 10 kcal mol<sup>-1</sup> Å<sup>-2</sup> for each simulation. Shift values of > 2.4 Å were not sampled as we believe that they are not realized in properly folded proteins. Free energy values for such shifts would also be affected by erroneous contributions from artificial exposition of hydrophobic surfaces at the ends of the inter-HAMP model. The system was modeled for at least 20 ns around each position. As the protomers are absolutely identical, the resulting free energy should also be symmetric as a function of the longitudinal shift. Thus, convergence was postulated if the energy difference between symmetrical positions (shifts of the same absolute value, but different signs) was less than 0.2 kcal/mol.

**HAMP Domain Axis Calculation.** To calculate the HAMP domain axis, the directions of helices AS1 and AS2 of both protomers were averaged.

**Protonation State of the Ionizable Residues.** On the basis of the data describing the environmental pH (25) as well as the optimal pH for enzymes from halophilic archaea (26), we expect the inner-cell pH to be in the range of 7.0–9.0. To make the correct choice of protonation states of ionizable residues, their  $pK_a$  values were predicted in corresponding environments. Predictions were performed with the MCCE2 multiconformation continuum electrostatics package (27).

In the NpHtrII HAMP domain region model (number 10 in Table S1 of the Supporting Information), 98 residues in both protomers were treated as ionizable. Multiple conformers for these residues were built with the total number of conformers being 5247. A conformer is defined as a heavy atoms rotamer of a certain side chain, in which protons are added, their positions are optimized, and a certain ionization state is chosen. Many conformers were included into the prediction because conformer sampling improves the match between experiment and calculation for individual residues and dramatically weakens the dependence on the starting structure (26). For our system, no residues were found to have a  $pK_a$  value in the range of 7–11 (see Table S2 of the Supporting Information). Therefore, all residues in the initial models of this simulation were left in their default protonation states.

We also studied the possibility of protonation–deprotonation events during the simulation of the NpHtrII inter-HAMP region.  $pK_a$  values of the key rechargeable residues (D137, R142, and D144) were predicted along the PMF trajectories. These residues, along with the non-rechargeable Q149, were subjected to extensive multiconformer trials, corresponding to different rotamers and ionization states. Conformers for other residues did not include side chain rotamers, only different ionization states. The total number of conformers was approximately 200–300 for different snapshots of the trajectory. Calculations were performed for the simulation at a molarity of 0.5 M, because at higher molarities  $pK_a$  shifts caused by solvation contributions would be even weaker, as follows from the Debye–Huckel theory of solvation. The total length of this simulation was 140 ns, and snapshots were taken every 200 ps. Resulting  $pK_a$  values, computed as a probability density function along the PMF trajectory, are given in Figure S1 of the Supporting Information. Briefly, for both D137 and D144, peaks of their distributions were shifted from the  $pK_a$  value in solution (3.71) not more than 0.1, with standard deviations of ~0.65 for D144 and ~0.42 for D137. In the case of R142, the peak of its  $pK_a$  distribution is shifted from the  $pK_a$  value in solution (12.1) to 13.1 with a standard deviation of 0.4. No points were observed in the pH range of 7–11. Therefore, the probability of the key residue switching its default protonation state is negligibly small under physiological conditions (pH 7.0–9.0).

## RESULTS

**Predictions of Structure for Inter-HAMP Regions.** We used the PSIPRED protein structure prediction server (28) to analyze sequences of studied proteins. For all of them, an  $\alpha$ -helical structure is predicted with a high degree of confidence for sequence fragments that consecutively include helix AS2 of the first HAMP domain, the inter-HAMP region, and helix AS1 of the second HAMP domain. The same fragments are predicted to

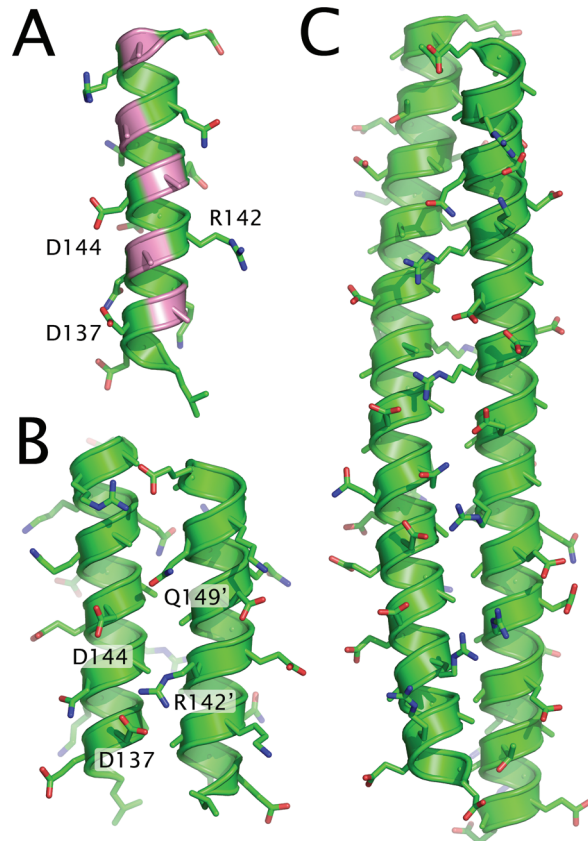


FIGURE 2: Proposed models for the inter-HAMP region. (A) Hydrophobic groove of the NpHtrII inter-HAMP fragment of residues 135–153. Alanines are highlighted in pink. (B) Structure of a homodimer of the two NpHtrII inter-HAMP regions of residues 135–153. Note the asymmetric position of protomers and the differences in ionic bonds formed on each side of the structure. (C) Structure of a homodimer of the two HsHtrII inter-HAMP regions of residues 356–400. Positions of the protomers are also asymmetric. The structure presented in panel A was determined by NMR [PDB entry 2RM8 (9)]. Panels B and C show manually built models, subjected to molecular dynamics.

be in a coiled coil by the coiled-coil prediction server (29) (Figure S2 of the Supporting Information).

**Model for Inter-HAMP Regions.** All inter-HAMP regions studied in this work have a pronounced continuous hydrophobic groove when modeled as an  $\alpha$ -helix (see that of NpHtrII, for example, in Figure 2A). Interestingly, this groove is composed mostly of alanines. Two identical fragments, modeled as ideal  $\alpha$ -helices in PyMOL and located so that the interface is at the hydrophobic groove, form a CC structure in <100 ps for the short inter-HAMP region of residues 135–153 of NpHtrII (Figure 2B), and <1 ns for the longer inter-HAMP regions of residues 356–400 of HsHtrII (Figure 2C) and residues 106–150 of HsHtrI. After formation of the CC, the structure remains stable during the whole length of the simulation (see Table S1 and Figures S6–S8 of the Supporting Information for additional information). In the longer inter-HAMP regions, deviations from the ideal  $\alpha$ -helical geometry are clearly seen, which is typical for CCs. The helices are bent around each other, with a total twist of 90° (Figure 2C). The twist is defined as the angle between projections of the lines, connecting the beginnings and ends of  $\alpha$ -helices, on the plane perpendicular to the CC axis (see Figure S3 of the Supporting Information for examples).

For all the modeled inter-HAMP regions, the homodimer adopts the asymmetric conformation, with a longitudinal shift of

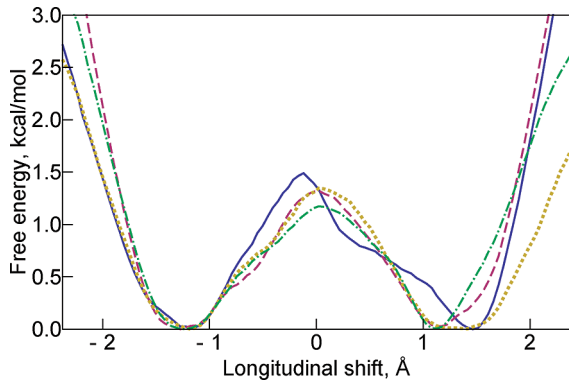


FIGURE 3: Free energy profiles for the relative longitudinal shift of the protomers in the inter-HAMP region (NpHtrII residues 135–153) at different molarities: 0.5 M (blue, solid), 1 M (magenta, dashed), 2 M (yellow, dotted), and 4 M (green, dotted–dashed). Note that the minima are at approximately  $\pm 1.3 \text{ \AA}$ , and the barrier height is 1.2–1.5 kcal/mol. For the sampling distributions and further information, see Figure S4 of the Supporting Information.

one protomer relative to the other of  $\sim 1 \text{ \AA}$ . The reason for this is most clear in the case of NpHtrII. Charged residues framing the hydrophobic core are distributed in such a way that the shifted conformation is preferred (Figure 2B). Namely, the positively charged R142' may be electrostatically attracted either by the negatively charged D137 or by the negatively charged D144. Simulations show that the conformation in which R142' is attracted by both D137 and D144 is unstable. Attraction of R142' in one protomer to D137 in the other leads to a longitudinal displacement, such that R142 comes closer to D144', and vice versa. The resulting shift is additionally stabilized by short-lived bonds between Q149' and D144. Designations without a prime correspond to one protomer, and those with a prime correspond to the other.

For a quantitative description of the inter-HAMP region, we calculated free energy profiles for the longitudinal shift using the umbrella sampling and weighted histogram analysis method (Figure 3; sampling distributions are presented in Figure S4 of the Supporting Information). Energy minima are observed at approximately  $\pm 1.3 \text{ \AA}$ . The barrier height is slightly different for different molarities, namely, 1.5 kcal/mol for 0.5 M, 1.4 kcal/mol for 1 and 2 M, and 1.2 kcal/mol for 4 M. These differences fall within the expected error of the method.

We believe that the observed features are not artifacts of the calculation, as we used the standard force field (CHARMM27). There are no regions with a high induced electronic polarization in the inter-HAMP region, so effects of different force fields on the obtained PMF profile were not addressed, as is sometimes done for free energy calculations of ion conduction through channels or for calculations of small ligand binding affinities. Weak variability of the free energy profile within the wide ion concentrations range also reflects the robustness of the observed features.

To check for possible systematic errors introduced by WHAM and to estimate statistical errors, we recalculated the free energy profiles using the multiple-Bennett acceptance ratio method (MBAR) (24). This method gave similar results (see Figure S4 of the Supporting Information for the corresponding graphs).

Therefore, we conclude that the observed asymmetry is not a calculation artifact.

**HAMP Domains.** To check the correspondence of the NMR HAMP domain structure (8) with those of Htrs, we modeled both HAMP domains of NpHtrII (residues 85–134 and 155–210 accordingly), along with the original HAMP domain of putative

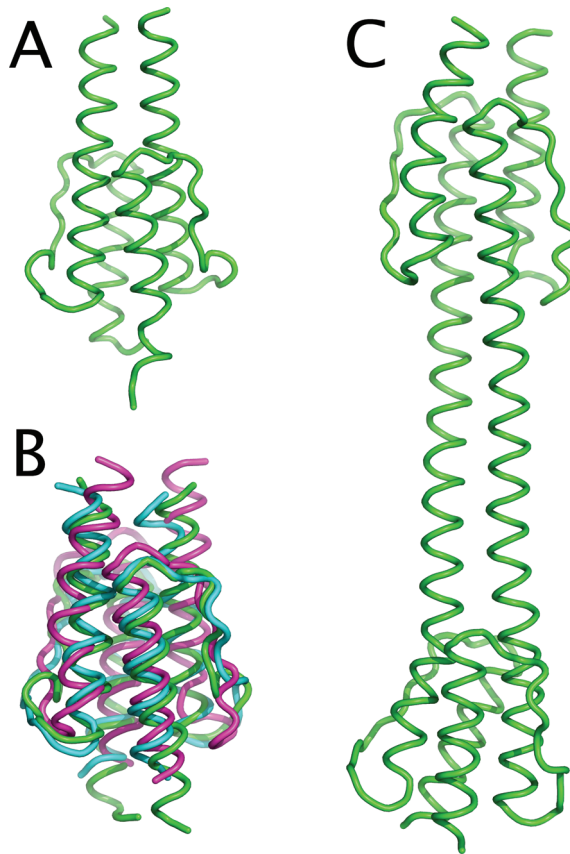


FIGURE 4: (A) Ribbon diagram of the Af1503 HAMP domain, expanded by the seven terminal amino acids, after molecular dynamics for 8 ns. (B) Overlay of the initial NMR structure of the Af1503 HAMP domain (green) with homology-modeled structures of the first (blue) and second (purple) NpHtrII HAMP domains. (C) Proposed model for the NpHtrII HAMP domain region (residues 85–210), including both HAMP domains and the inter-HAMP region. Note the asymmetry between the protomers and the tilt of the axes of the HAMP domains relative to the axis of the inter-HAMP region.

protein Af1503 of *A. fulgidus*. Initial models generated by MODELLER were equilibrated for 4 ns and appeared to be very stable. The NMR model (PDB entry 2ASW) of the Af1503 HAMP domain, containing residues 276–331, was later expanded by residues 332–338 (amino acids SLEEALK), modeled as an  $\alpha$ -helical continuation of AS2. These last seven residues of Af1503 were not included in the construct for the determination of the NMR structure but could somehow influence the structure of the HAMP domain. The resulting expanded structure was also stable for 8 ns. The average root-mean-square deviations (rmsd) for the backbone atoms during the simulations were 1.5  $\text{\AA}$  for HAMP1 of NpHtrII, 1.7  $\text{\AA}$  for HAMP2 of NpHtrII, 1.4  $\text{\AA}$  for the Af1503 fragment of residues 276–331, and 1.6  $\text{\AA}$  for the Af1503 fragment of residues 276–331. A more extensive stability analysis is given in the Supporting Information. Ribbon diagrams of the resulting structures are presented in Figure 4A,B.

**Modeling of the HAMP Domains with the Inter-HAMP Region.** To check whether the structure of the HAMP domain is affected by the inter-HAMP region or vice versa, we performed molecular dynamics studies for two constructs. HAMP1 with the inter-HAMP region of NpHtrII (residues 85–153) were simulated for 10 ns, and HAMP1, the inter-HAMP region, and HAMP2 of NpHtrII (residues 85–210) were simulated for 60 ns. Though large structural movements are seen, they do not change the architecture

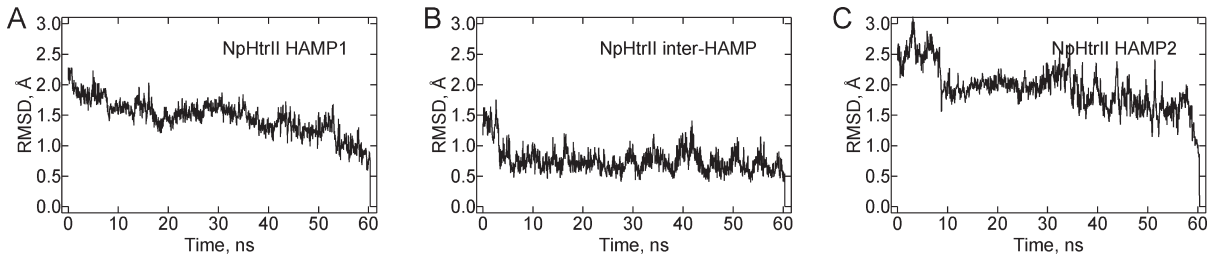


FIGURE 5: Root-mean-square deviations for different parts of the NpHtrII HAMP domain region, simulated as a whole. Only the backbone atoms are included in the calculation. For each part, the last trajectory snapshot was used as a reference structure. See the Supporting Information for more detail.

of these constructs. Root-mean-square deviations for the whole NpHtrII HAMP domain region are presented in Figure 5. To calculate rmsds, the last trajectory snapshot was used as a reference structure. Only the backbone atoms were included in the calculation. An extensive stability analysis for this construct is given in Table S1 and Figures S13–S17 of the Supporting Information. Despite the initial symmetrical conformation of the system, a relative longitudinal shift of corresponding  $\alpha$ -helices develops after a few nanoseconds and persists for the whole length of the simulation. As opposed to the zero twist angle of the inter-HAMP region alone, it equals approximately  $45^\circ$  in the presence of the HAMP domains. The twist is defined above and explained in more detail in Figure S3 of the Supporting Information. HAMP domains themselves retain their general conformations (Figures S16 and S17 of the Supporting Information). However, the shift imposed by the inter-HAMP region results in a reorientation of corresponding helices and renders HAMPs highly asymmetric (Figure 4C and Figures S16 and S17 of the Supporting Information). The relative position of the two HAMP domains changes considerably, though the directions of the main axes of both HAMP domains coincide well with each other. The angle between the axes of HAMP1 and HAMP2 is  $9 \pm 5^\circ$ , as opposed to  $13 \pm 4^\circ$  for the angle between HAMP1 and the inter-HAMP region and  $16 \pm 6^\circ$  for the angle between HAMP2 and the inter-HAMP region.

As we suppose that transmembrane helices TM2 and TM2' may continue in HAMP1 helices AS1 and AS1' without a kink (see a hypothetical model in Figure S5 of the Supporting Information), we considered it interesting to analyze the motion of HAMP2 relative to the membrane plane and to the transmembrane segment of NpHtrII. For this purpose, we calculated the probability density of the projection of the HAMP2 center of mass (COM) on the membrane plane relative to the HAMP1 COM (Figure 6, including a symmetrical image that corresponds to the longitudinal shift with the opposite value). The probability density distribution function was determined as the time that the projection of the second HAMP domain's center of mass onto the membrane plane spent in a given  $1 \text{ \AA} \times 1 \text{ \AA}$  square, divided by the total simulation time. The distance between the projections of the centers of mass of the two HAMP domains is  $8.6 \pm 3.5 \text{ \AA}$ . This value is approximately equal to what follows from simple geometric considerations: the length of the inter-HAMP region is approximately  $50 \text{ \AA}$ , the mean distance between centers of the helices is  $9 \text{ \AA}$ , the mean longitudinal shift value is  $1.3 \text{ \AA}$ , and thus the in-plane displacement is  $\sim 7 \text{ \AA}$  (Figure 7C).

## DISCUSSION

Herein, we have reported the model of the inter-HAMP region of sensory rhodopsin transducers. It is quite similar to the

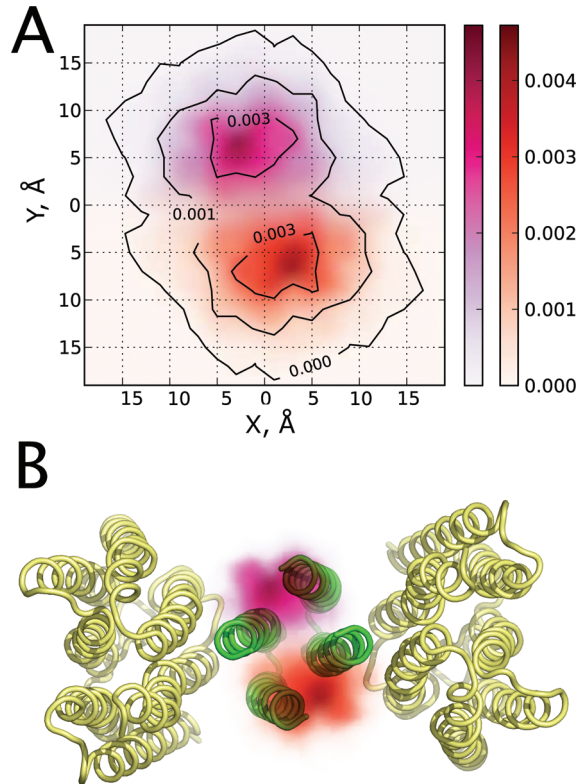
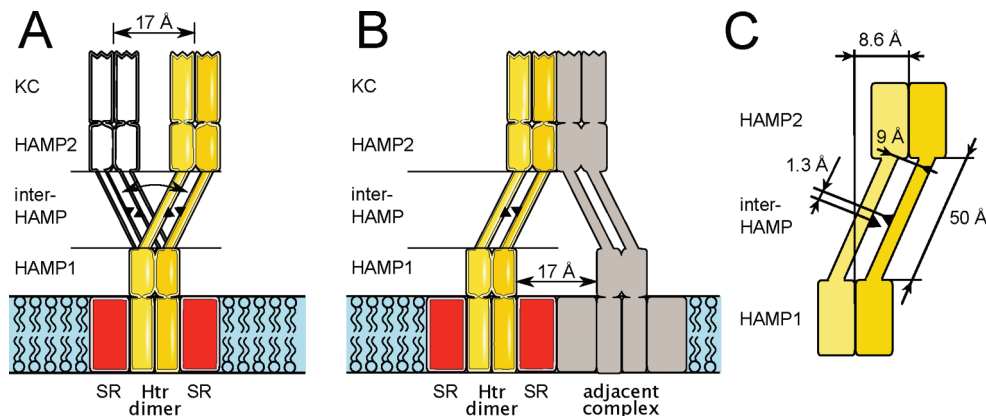


FIGURE 6: (A) Computed probability of finding the projection of the NpHtrII second HAMP domain center of mass on the membrane plane at the corresponding  $X$ ,  $Y$  coordinates, in inverse square angstroms. View from the cytoplasm. The  $X$  axis is directed along the centers of mass of the HAMP1 AS1 helices; the  $Y$  axis is perpendicular to it, and both axes lie in the membrane plane. The initial structure was symmetric, and the tilt and the longitudinal shift in the inter-HAMP region developed later. Two regions with the highest probability correspond to the two possible signs of longitudinal shifts and are colored red and magenta, correspondingly, to guide the eye. (B) Same probability density distribution laid over the structure of the 2:2 NpSRII–NpHtrII complex on a proper scale. PDB entry 1H2S (6).

signaling helix (S Helix) (30) in that it continues AS2 of the HAMP domain. The observed differences are as follows. First, at its C-terminus, the inter-HAMP region also ends with a HAMP domain helix (AS1). Second,  $a$  and  $d$  CC positions are occupied by alanines in the inter-HAMP region, as opposed to bulky amino acids of the S Helix. We expect that this may facilitate longitudinal motions of protomers along each other.

Molecular dynamics simulation shows that a symmetric conformation of the inter-HAMP domain is unfavorable. A longitudinal shift between the inter-HAMP protomers is observed. Because they are identical, a longitudinal shift of the same value



**FIGURE 7:** Two possible roles of the HAMP domain region of phototactic signal transducers. The model of the 2:2 sensory rhodopsin-transducer complex is colored yellow, with the protomers shown in different shades. Equivalent positions are marked on the inter-HAMP regions of the two protomers as black triangles to facilitate the perception of the longitudinal shift. (A) The change in the sign of the longitudinal shift results in a distinct conformation, in which the kinase control module (KC) is displaced on average by  $8.6 \text{ \AA} \times 2$  ( $\approx 17 \text{ \AA}$ ) along the membrane plane (second conformation colored white). Thus, the signal may be transduced through the inter-HAMP switching. (B) Asymmetry of the HAMP domain region may facilitate the contacts with the adjacent transducers or receptors. Otherwise, these contacts would be impaired by bulky sensory rhodopsins, residing in the membrane. (C) Simple geometrical model of the conversion of the inter-HAMP longitudinal shift in the displacement of the transducer's cytoplasmic part. Data presented are the mean values. The mean displacement of the second HAMP domain relative to the first one in the membrane plane is  $8.6 \text{ \AA}$ . The approximate length of the inter-HAMP region is  $50 \text{ \AA}$ . The approximate distance between the axes of the inter-HAMP helices is  $9 \text{ \AA}$ . The mean longitudinal shift in the inter-HAMP region is  $1.3 \text{ \AA}$ .

but of the opposite sign is also possible. It means that the inter-HAMP region is bistable. The energetic barrier between the two states is sufficiently high to prevent frequent switching by thermal fluctuations, but it is much lower than  $60 \text{ kcal/mol}$ , the average energy of the photons, absorbed by sensory rhodopsins. An asymmetric conformation of the inter-HAMP region persists when the HAMP domains are also included in the simulation. We suggest that this is biologically relevant. It is important to note that the asymmetry of the inter-HAMP region is coupled with the asymmetry of the HAMP domains.

The established properties of the inter-HAMP region may have direct implications for our understanding of the signal propagation through the cytoplasmic part of the transducers. As the inter-HAMP  $\alpha$ -helices constitute a CC and are always turned to each other by their hydrophobic groove, signaling through the changes in the interhelical angle as supposed in ref 8 is questionable. We suggest that the probable mechanism of signal transduction may involve either switching of the inter-HAMP region or some rigid body motion of the cytoplasmic part without any changes in the inter-HAMP state (Figure 7). Switching might result in a large structural rearrangement (Figure 7A) and thus could be prohibited by tight hexagonal packing of KC fragments. Signal encoding by displacement of the whole cytoplasmic part of the transducer, i.e., by a position of HAMP2 relative to HAMP1, in turn would be affected by very large fluctuations (Figure 6A,B).

As we have noted, asymmetry of the inter-HAMP is enforced by electrostatic interactions of oppositely charged side chains of corresponding residues. Flexibility of those side chains allows some longitudinal displacements (up to zero shift) without breaking of the formed electrostatic bonds. Thus, the evolution of the system with time may be different depending on which bonds are formed, that is, the history of the system. This means that the inter-HAMP region is in effect a multistate switch. It is worth mentioning that a study of the HAMP domain alone would not provide sufficient information about signal transduction.

## CONCLUSION

We built a model of the inter-HAMP region and of the flanking HAMP domains and studied their structure and properties via

molecular dynamics. It was found that the Htr inter-HAMP region forms a CC. The structure is asymmetric, as there is a longitudinal shift of protomers of  $\sim 1.3 \text{ \AA}$ . HAMP domains are mechanistically coupled to the inter-HAMP region and are also asymmetric. Taking all described features into consideration, we propose the following functions for the inter-HAMP regions. First, they impose an initially asymmetric conformation on the Htr dimer, which may help to bring kinase control fragments sufficiently close in space to come into contact [in membranes, the Htr dimer is surrounded by two sensory rhodopsins, and thus, Htr dimer centers are separated by at least  $30 \text{ \AA}$  (6) (see Figure 6B)]. Second, they may act as a switch, which needs no signal input to maintain its state but changes its output upon receiving a proper signal.

## ACKNOWLEDGMENT

I.Yu.G. is thankful to the Institut de Biologie Structurale J.-P. Ebel and to the Institute of Structural Biology and Biophysics (ISB-2) for providing excellent conditions for his work during his visits.

## SUPPORTING INFORMATION AVAILABLE

Full description of the molecular models presented in this study, graph of the  $pK_a$  distribution of the important NpHtrII inter-HAMP ionizable residues, sequence alignment of the HAMP domain regions, secondary structure and CC prediction data for HsHtrI, HsHtrII, and NpHtrII, a figure explaining the definition of the twist angle, separate NpHtrII inter-HAMP domain PMF plots with error bars and umbrella sampling distribution histograms, the hypothetical model of the junction between the NpHtrII HAMP domain and its transmembrane segment, rmsd graphs for all the HAMP domains and the inter-HAMP region modeled in this study, packing analysis of the NpHtrII HAMP domains as a part of the HAMP domain region, and a table of the  $pK_a$  values of ionizable residues in the NpHtrII HAMP domain region model. This material is available free of charge via the Internet at <http://pubs.acs.org>.

## REFERENCES

1. Klare, J., Chizhov, I., and Engelhard, M. (2008) Microbial Rhodopsins: Scaffolds for Ion Pumps, Channels, and Sensors. In *Bioenergetics*, pp 73–122, IRL Press at Oxford University Press, Oxford, U.K.
2. Sasaki, J., and Spudich, J. L. (2008) Signal Transfer in Haloarchaeal Sensory Rhodopsin-Transducer Complexes. *Photochem. Photobiol.* **84**, 863–868.
3. Hazelbauer, G. L., Falke, J. J., and Parkinson, J. S. (2008) Bacterial chemoreceptors: High-performance signaling in networked arrays. *Trends Biochem. Sci.* **33**, 9–19.
4. Aravind, L., and Ponting, C. P. (1999) The cytoplasmic helical linker domain of receptor histidine kinase and methyl-accepting proteins is common to many prokaryotic signalling proteins. *FEMS Microbiol. Lett.* **176**, 111–116.
5. Moukhambetianov, R., Klare, J. P., Efremov, R., Baeken, C., Goppner, A., Labahn, J., Engelhard, M., Büldt, G., and Gordeliy, V. I. (2006) Development of the signal in sensory rhodopsin and its transfer to the cognate transducer. *Nature* **440**, 115–119.
6. Gordeliy, V. I., Labahn, J., Moukhambetianov, R., Efremov, R., Granzin, J., Schlesinger, R., Büldt, G., Savopol, T., Scheidig, A. J., Klare, J. P., and Engelhard, M. (2002) Molecular basis of transmembrane signalling by sensory rhodopsin II-transducer complex. *Nature* **419**, 484–487.
7. Etzkorn, M., Seidel, K., Li, L., Martell, S., Geyer, M., Engelhard, M., and Baldus, M. (2010) Complex Formation and Light Activation in Membrane-Embedded Sensory Rhodopsin II as Seen by Solid-State NMR Spectroscopy. *Structure* **18**, 293–300.
8. Hulkko, M., Berndt, F., Gruber, M., Linder, J. U., Truffault, V., Schultz, A., Martin, J., Schultz, J. E., Lupas, A. N., and Coles, M. (2006) The HAMP Domain Structure Implies Helix Rotation in Transmembrane Signaling. *Cell* **126**, 929–940.
9. Hayashi, K., Sudo, Y., Jee, J., Mishima, M., Hara, H., Kamo, N., and Kojima, C. (2007) Structural Analysis of the Phototactic Transducer Protein HtrII Linker Region from *Natronomonas pharaonis*. *Biochemistry* **46**, 14380–14390.
10. Kim, K. K., Yokota, H., and Kim, S. (1999) Four-helical-bundle structure of the cytoplasmic domain of a serine chemotaxis receptor. *Nature* **400**, 787–792.
11. Chervitz, S. A., and Falke, J. J. (1996) Molecular mechanism of transmembrane signaling by the aspartate receptor: A model. *Proc. Natl. Acad. Sci. U.S.A.* **93**, 2545–2550.
12. Falke, J. J., and Erbse, A. H. (2009) The Piston Rises Again. *Structure* **17**, 1149–1151.
13. Ames, P., Zhou, Q., and Parkinson, J. S. (2008) Mutational Analysis of the Connector Segment in the HAMP Domain of Tsr, the *Escherichia coli* Serine Chemoreceptor. *J. Bacteriol.* **190**, 6676–6685.
14. Zhou, Q., Ames, P., and Parkinson, J. S. (2009) Mutational Analyses of HAMP Helices Suggest a Dynamic Bundle Model of Input-Output Signaling in Chemoreceptors. *Mol. Microbiol.* **73**, 801–814.
15. Airola, M. V., Watts, K. J., Bilwes, A. M., and Crane, B. R. (2010) Structure of Concatenated HAMP Domains Provides a Mechanism for Signal Transduction. *Structure* **18**, 436–448.
16. The UniProt Consortium (2010) The Universal Protein Resource (UniProt) in 2010. *Nucleic Acids Res.* **38**, D142–D148.
17. Sali, A., and Blundell, T. L. (1993) Comparative protein modelling by satisfaction of spatial restraints. *J. Mol. Biol.* **234**, 779–815.
18. Grudinin, S., and Redon, S. (2010) Practical modeling of molecular systems with symmetries. *J. Comput. Chem.* **31**, 1799–1814.
19. Phillips, J. C., Braun, R., Wang, W., Gumbart, J., Tajkhorshid, E., Villa, E., Chipot, C., Skeel, R. D., Kale, L., and Schulten, K. (2005) Scalable molecular dynamics with NAMD. *J. Comput. Chem.* **26**, 1781–1802.
20. MacKerell, A. D., Jr., Bashford, D., Bellott, M., Dunbrack, R. L., Jr., Evanseck, J. D., Field, M. J., Fischer, S., Gao, J., Guo, H., Ha, S., Joseph-McCarthy, D., Kuchnir, L., Kuczera, K., Lau, F. T. K., Mattos, C., Michnick, S., Ngo, T., Nguyen, D. T., Prodhom, B., Reiher, W. E., III, Roux, B., Schlenkrich, M., Smith, J. C., Stote, R., Straub, J., Watanabe, M., Wiorkiewicz-Kuczera, J., Yin, D., and Karplus, M. (1998) All-Atom Empirical Potential for Molecular Modeling and Dynamics Studies of Proteins. *J. Phys. Chem. B* **102**, 3586–3616.
21. Humphrey, W., Dalke, A., and Schulten, K. (1996) VMD: Visual molecular dynamics. *J. Mol. Graphics* **14**, 33–38.
22. Frenkel, D., and Smit, B. (2002) Understanding molecular simulation: From algorithms to applications, Academic Press, New York.
23. Kumar, S., Rosenberg, J. M., Bouzida, D., Swendsen, R. H., and Kollman, P. A. (2004) Multidimensional free-energy calculations using the weighted histogram analysis method. *J. Comput. Chem.* **16**, 1339–1350.
24. Shirts, M. R., and Chodera, J. D. (2008) Statistically optimal analysis of samples from multiple equilibrium states. *J. Chem. Phys.* **129**, 124105.
25. Falb, M., Pfeiffer, F., Palm, P., Rodewald, K., Hickmann, V., Tittor, J., and Oesterhelt, D. (2005) Living with two extremes: Conclusions from the genome sequence of *Natronomonas pharaonis*. *Genome Res.* **15**, 1336–1343.
26. Cao, Y., Liao, L., Xu, X. W., Oren, A., and Wu, M. (2008) Aldehyde dehydrogenase of the haloalkaliphilic archaeon *Natronomonas pharaonis* and its function in ethanol metabolism. *Extremophiles* **12**, 849–854.
27. Song, Y., Mao, J., and Gunner, M. R. (2009) MCC2E: Improving protein pK<sub>a</sub> calculations with extensive side chain rotamer sampling. *J. Comput. Chem.* **30**, 2231–2247.
28. McGuffin, L. J., Bryson, K., and Jones, D. T. (2000) The PSIPRED protein structure prediction server. *Bioinformatics* **16**, 404–405.
29. Lupas, A., Van Dyke, M., and Stock, J. (1991) Predicting coiled coils from protein sequences. *Science* **252**, 1162–1164.
30. Anantharaman, V., Balaji, S., and Aravind, L. (2006) The signaling helix: A common functional theme in diverse signaling proteins. *Biol. Direct* **1**, 25.